Research article

E44Q mutation in Na$_V$1.7 in a patient with infantile paroxysmal knee pain: electrophysiological analysis of voltage-dependent sodium current

Kiichi Takahashi [a], Takayoshi Ohba [b], Yosuke Okamoto [b], Atsuko Noguchi [a], Hiroko Okuda [c], Hatasu Kobayashi [d], Kouji H. Harada [e], Akio Koizumi [f], Kyoichi Ono [b], Tsutomu Takahashi [a,*]

[a] Department of Pediatrics, Akita University Graduate School of Medicine, 1-1-1, Hondo, Akita City, Akita, 010-8543, Japan
[b] Department of Cell Physiology, Akita University Graduate School of Medicine, 1-1-1, Hondo, Akita City, Akita, 010-8543, Japan
[c] Department of Pain Pharmacogenetics, Kyoto University Graduate School of Medicine, Yoshida Konoe, Sakyo, Kyoto, 606-8501, Japan
[d] Department of Environmental and Molecular Medicine, Mie University Graduate School of Medicine, 2-174 Edobashi, Tsu, Mie, 514-8507, Japan
[e] Department of Health and Environmental Sciences, Kyoto University Graduate School of Medicine, Yoshida Konoe, Sakyo, Kyoto, 606-8501, Japan
[f] Institute of Public Health and Welfare Research, 18-13, Uzumasa Tanamori, Ukyo, Kyoto, 616-8141, Japan

A R T I C L E I N F O

A B S T R A C T

Gain-of-function mutations in voltage-gated sodium channels (Na$_V$1.7, Na$_V$1.8, and Na$_V$1.9) are known causes of inherited pain disorders. Identification and functional assessment of new Na$_V$1.7 mutations could help elucidate the phenotypic spectrum of Na$_V$1.7 channelopathies. We identified a novel Na$_V$1.7 mutation (E44Q in exon 2) that substitutes a glutamic acid residue for glutamine in the cytoplasmic N-terminus of Na$_V$1.7 in a patient with paroxysmal pain attacks during childhood and his family who experienced similar pain episodes. To study the sodium channel's function, we performed electrophysiological recordings. Voltage-clamp recordings revealed that the mutation increased the amplitude of the non-inactivating component of the sodium current, which might facilitate channel opening. These data demonstrate that E44Q is a gain-of-function mutation in Na$_V$1.7, which is consistent with our patient's pain phenotype.

1. Introduction

Voltage-gated sodium channels are essential for triggering electrical signaling in nerves, muscles, and endocrine cells [1]. Voltage-gated sodium channels consist of an α subunit and β subunits. An α subunit of 260 kDa forms a pore, which can be coupled to β subunits of 30–40 kDa. In humans and other mammals, α subunits are encoded by 10 genes, nine of which (Na$_V$1.1–1.9) are voltage-gated. Na$_V$1.7, Na$_V$1.8, and Na$_V$1.9 (encoded by *SCN9A*, *SCN10A*, and *SCN11A*, respectively) are strongly expressed in sensory neurons [2].

Genetic and genomic sequencing and electrophysiological recordings have revealed a relationship between human pain disorders and voltage-gated sodium channel mutations in *SCN9A*, *SCN10A*, and *SCN11A* [3, 4, 5, 6]. We previously identified *SCN11A* mutations in patients with familial episodic limb pain (FEP) [7]. Patients with FEP have episodic paroxysmal limb pain that is induced by cold, rainy weather during childhood and may decrease during adolescence [8]. In *SCN9A*, loss-of-function mutations result in congenital insensitivity to pain. Heterozygous mutations in *SCN9A* cause inherited erythromelalgia

(IEM) and paroxysmal extreme pain disorder (PEPD). IEM results in a paroxysmal burning sensation and erythema in the arms and legs [9, 10], and PEPD is associated with severe pain in the proximal regions of the body [11, 12]. Electrophysiological experiments have revealed that IEM-linked *SCN9A* mutations produce a hyperpolarizing shift in voltage-dependent activation, increase the ramp current, and cause slow deactivation leading to dorsal root ganglion (DRG) neuron hyperexcitability [13, 14, 15, 16, 17]. Conversely, PEPD-linked *SCN9A* mutations shift voltage-dependent steady-state fast inactivation towards depolarization, sometimes producing a persistent current, leading to increased DRG neuron excitability [18, 19].

Here, we report a novel mutation in the N-terminus of Na$_V$1.7 (E44Q) in a patient with childhood paroxysmal knee pain that disappeared during adulthood. The disease resembled *SCN11A*-linked FEP more rather than other *SCN9A*-related pain disorders. Using voltage-clamp techniques, we showed that this gain-of-function mutation increased the non-inactivating component of sodium currents induced by a ramp-pulse protocol, leading to the pain phenotype experienced by the proband.

---

* Corresponding author.
E-mail address: tomy@med.akita-u.ac.jp (T. Takahashi).

2. Material and methods

2.1. Patients and genomic DNA isolation

Blood samples were obtained from the proband and his relatives, and genomic DNA was isolated from the white blood cells using the QIAamp DNA Blood Mini Kit (Qiagen, Hilden, Germany).

2.2. Exon screening and SCN9A mutation analysis

Whole-exome sequencing of the proband was performed. The target exonic regions and flanking intronic regions were captured by the SureSelect Human All Exon V4+UTR Kit (Agilent Technologies, Santa Clara, CA, USA), and sequenced on the Illumina HiSeq 2000 platform (Illumina Inc., San Diego, CA, USA). Sequence data were mapped to the hg19 genomic location (University of California Santa Cruz Genome Browser hg19; http://hgdownload.cse.ucsc.edu/goldenPath/hg19/chromosomes/) with Burrows-Wheeler Aligner software (version 0.6.2; http://bio-bwa.sourceforge.net/index.shtml). Small insertions/deletions and single-nucleotide variants were found using the Genome Analysis Toolkit software (version 1.6–13; https://www.broadinstitute.org/gatk/). To identify candidate variants, the data were filtered using a previously described method [8]. The mutations were confirmed using Sanger sequencing. The primers are listed in Table 1.

2.3. Cell culture and transfection

Human embryonic kidney 293T (HEK293T) cells were seeded on 9-mm glass coverslips and cultured in humidified air and 5% CO_2 at 37 °C. The culture medium was Dulbecco's modified Eagle's medium (DMEM; Fuji Film Wako Pure Chemical Corporation, Osaka, Japan) with 10% heat-inactivated fetal bovine serum, 4 mmol/l L-glutamine, and 1% penicillin/streptomycin. Plasmids expressing either wild-type (WT) SCN9A or E44Q SCN9A were transiently transfected together with SCN1B plus SCN2B into HEK293T cells using Lipofectamine 2000 (Thermo Fisher Scientific, Waltham, MA, USA).

2.4. Electrophysiological recordings

Two days following successful transfection, we performed whole-cell voltage-clamp recordings at 25 °C using appropriate emission filters, ACT-2U control software (version 1.70; Nikon Instruments, Tokyo, Japan), and the DS-5Mc DS Cooled Camera Head (Nikon Instruments) mounted on a Nikon Eclipse TE2000-U Inverted Microscope (Nikon Instruments). Microelectrodes were pulled from borosilicate glass (1.50 mm/1.10 mm, outer diameter/inner diameter; Warner Instruments, Hamden, CT, USA). Electrodes were fabricated using a P-97 Flaming/Brown type micropipette puller (Sutter Instrument, Novato, CA, USA) and had resistances of 2–5 MΩ when filled with the pipette solution. Standard whole-cell currents were filtered at 2 kHz, recorded at 10 or 100 kHz using an Axopatch 200B amplifier controlled by Clampex software (Molecular Devices, San Jose, CA, USA), and digitized using Digidata 1322A (Axon Instruments, Union City, CA, USA). The pipette potential was adjusted to zero before seal formation. Capacity transients were canceled, and the voltage errors were minimized with 80–90% series resistance compensation. The bath solution contained (in mM): 40 NaCl, 3 KCl, 100 Tris-HCl, 1 $CaCl_2$, 1 $MgCl_2$, 10 HEPES, and 10 glucose (pH 7.4 with Tris base) at the activation measure; or 140 NaCl, 3 KCl, 1 $CaCl_2$, 1 $MgCl_2$, 10 HEPES, and 10 glucose (pH 7.4 with NaOH) at the

inactivation measure. The pipette solution contained (in mM): 140 CsF, 10 NaCl, 1 EGTA, and 10 HEPES (pH 7.3 with CsOH).

Whole-cell configuration was established, and after an equilibration period of 5 min, the recordings began. To assess the current-voltage (I–V) relationship, cells were held at −120 mV. Then, the voltage was subjected to various test pulses ranging from −120 to +40 mV in 5 mV increments for 20 ms. The inter-sweep interval was 1 s. The maximal amplitude of sodium inward currents was measured, normalized with the cell capacitance, and plotted as a function of test voltage to generate the I–V plot, including a regression line between +10 and +40 mV. Decaying currents were fit with a single-exponential equation of the form as follows:

$$I = A * \exp\left(-\frac{t}{\tau}\right) + I_c \tag{1}$$

where A, t, τ, and Ic indicate the amplitude of the fit, time, time constant of decay, and asymptotic minimum to which the currents decay, respectively. The reversal potential of sodium current (V_{rev}) was determined by extrapolating the regression line to the transverse axis, and peak sodium conductance (G_{max}) was obtained from the slope of this line. The activation curves were obtained by converting I to conductance (G) at each voltage (V) using the equation

$$G = I / (V - V_{rev}) \tag{2}$$

The activation curves were then fitted to the Boltzmann function as shown below.

$$G / G_{max} = 1 / \{1 + \exp[(V\frac{1}{2} - V) / k]\} \tag{3}$$

G_{max}, $V_{1/2}$, and k indicate the maximum conductance, midpoint of the activation curve, and slope factor, respectively. The measurement of the steady-state inactivation of sodium current was conducted both for fast and slow inactivation [13]. For the fast inactivation, the peak amplitude at −10 mV test pulse with 40 ms duration was documented after a 500 ms prepulse ranging from −120 to −10 mV with 5 mV increments. The peak inward currents at the test pulse were normalized to the maximum current amplitude and plotted against the prepulse membrane voltage to construct the inactivation curve. The inactivation curve was then fitted to the Boltzmann function as follows:

$$I / I_{max} = 1 / \{1 + \exp[(V - V\frac{1}{2}) / k]\} \tag{4}$$

where I_{max}, $V_{1/2}$, and k indicate the maximum conductance, midpoint of fast inactivation, and slope factor, respectively. To determine the steady-state slow inactivation, 30-s prepulses were set up ranging from −120 mV to +20 mV with 10 mV increments followed by a 100-ms hyperpolarization to −120 mV. Cells were then depolarized to a −10 mV test pulse for 5 ms. Peak inward currents at the test pulse were normalized to the maximum current amplitude and fitted to the Boltzmann function as given below.

$$I / I_{max} = 1 / \{1 + \exp[(V - V\frac{1}{2}) / k]\} \tag{5}$$

I_{max}, $V_{1/2}$, and k indicate the maximum conductance, midpoint of slow inactivation, and slope factor, respectively. To evaluate the non-inactivating component of the sodium current, the ramp voltage-clamp pulses (dV/dt = 0.2 mV/ms) with 600 ms duration were applied from −100 to +20 mV to the cell at a frequency of 0.05 Hz. The current amplitude was normalized to the maximal peak inward current recorded during the activation protocol. We excluded data for WT and E44Q with peak currents of more than −1 nA to avoid insufficient voltage controls during voltage-clamp experiments.

2.5. Data analysis

Electrophysiological data were analyzed using Igor Pro 6.36 (Wave-Metrics, Portland, OR, USA), and the data are presented as mean ±

Table 1. Primers used for amplification of the SCN9A gene.

Exon	Forward Primer (5' > 3')	Reverse Primer (5' > 3')
2	TCTTGGCAGGCAAATAGTTAA	CAGAAGGAAGCCAACAGAAA

standard error. Statistical significance was determined by a two-sided Student's t-test or Mann–Whitney U-test, as appropriate. Statistical significance was calculated using SPSS Statistics 22.0.0 (SPSS Inc., Chicago, IL, USA) and set at p < 0.05.

2.6. Ethics approval and consent to participate

The clinical and genetic studies were approved by the Institutional Review Board and Ethics Committee of Akita University Graduate School of Medicine, Japan (approval no. 960; approval date, 26 September 2012) and the Kyoto University School of Medicine, Japan (approval no. G501; approval date, 2 August 2012). Written informed consent was obtained from the patient and his relatives prior to their participation in the study.

3. Results

3.1. Clinical description

A 53-year-old male patient had been experiencing episodes of paroxysmal knee pain since the age of 4. He had no prior medical history. The pain was dull and lasted for several hours to a few days, at a frequency of 4 times per year. The episodes of pain were induced by fatigue or by weather and seasonal changes, especially when the temperature and atmospheric pressure dropped, and never occurred in summer or on a hot day. Pain was relieved by warming.

Paroxysmal knee pain episodes started to decrease at the age of 12. However, trigeminal neuralgia and occipital neuralgia arose in his 20s. The pain lasted for a few hours to several days and improved with non-steroidal anti-inflammatory drugs. His father had experienced similar symptoms of knee pain in his childhood and had trigeminal neuralgia from the age of 50 years (Figure 1A).

3.2. Genetic analysis

Whole-exome analysis revealed no mutations in the coding regions of *SCN10A* and *SCN11A* after applying the selection criteria. A G to C substitution (c.130G > C) in exon 2 was found in the proband and his father, but not in his mother, by sequence analysis of *SCN9A* (Figure 1B). This single-nucleotide mutation caused the substitution of a glutamic acid residue with glutamine (E44Q) in the cytoplasmic N-terminus of $Na_V1.7$ (Figure 1B). Glutamic acid 44 is not conserved across all other members of the sodium channel family but is conserved across all $Na_V1.7$ orthologs from the different species known to date (Figure 1C). According to data from the 1000 Genomes Project database, this mutation is not found in the Japanese or any other population. This mutation has also not been detected in another Japanese variant database, the Human Genetic Variation Database. No rare or novel variant (allele frequency <0.05) was detected in $Na_V1.8$ or $Na_V1.9$.

3.3. Voltage-clamp characterization

To assess the effects of the E44Q mutation on the channel's gating properties, we recorded sodium currents from HEK293T cells transiently transfected with WT or $Na_V1.7$ harboring the E44Q mutation. Since half-maximal activation and half-maximal inactivation potentials were shifted to more negative potentials upon establishing the whole-cell configuration, the experiment was performed 5 min after establishing the whole-cell configuration. Figure 2A shows representative whole-cell current densities of WT (a) and E44Q (b) channels elicited with a series of depolarizing test pulses from a holding potential of −120 mV Figure 2B shows the peak current density-voltage relationship curves, and Figure 2C represents the inactivation time constants. Inactivation time constants were not significantly different between WT (n = 9) and E44Q (n = 8).

Voltage-dependent activation curves were obtained from the Boltzmann fits of normalized conductance (Figure 3A). The E44Q mutation did not affect the midpoint of activation (WT: $V_{1/2}$ = −24.6 ± 6.3 mV, k = 5.0 ± 1.1, n = 9; E44Q: $V_{1/2}$ = −25.3 ± 6.5 mV, k = 4.9 ± 0.9, n = 8; p = 0.847). Next, we assessed the effects of the E44Q mutation on the inactivation properties. Figure 3B shows fast-inactivation curves acquired from the Boltzmann fits to the normalized conductance. The voltage dependence of steady-state fast inactivation was shifted in the depolarizing direction by the E44Q mutation; however, it was not significantly different. The midpoint of fast inactivation ($V_{1/2}$, measured with 500 ms prepulses) was −83.4 ± 6.8 mV for WT (n = 9) and –79.4 ±
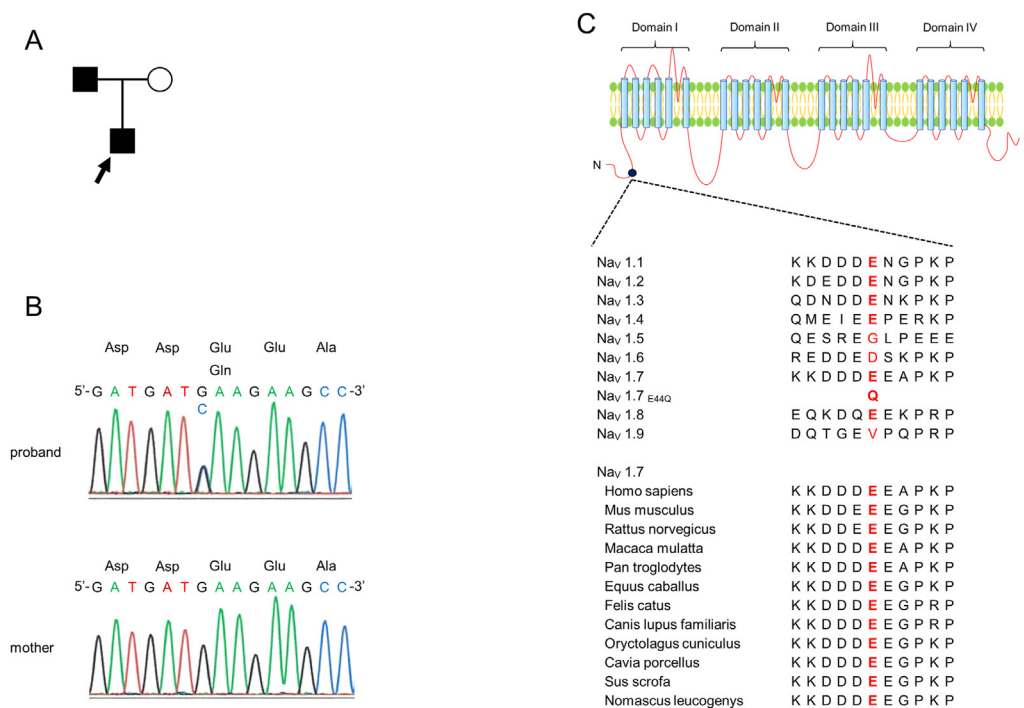

Figure 1. (A) Family pedigree representing the proband and his parents. Squares denote males, and circles denote females. The arrow indicates the proband. Filled symbols denote clinically affected individuals. (B) Sanger sequencing analysis of the *SCN9A* gene. The proband was heterozygous for the missense mutation c.130G > C (p.E44Q). The same mutation was present in his father but not his mother. (C) Sequence alignment of the N-terminus of voltage-gated sodium channels. The schematic of the topology of the sodium channel demonstrates the location of the E44Q mutation (black circle).
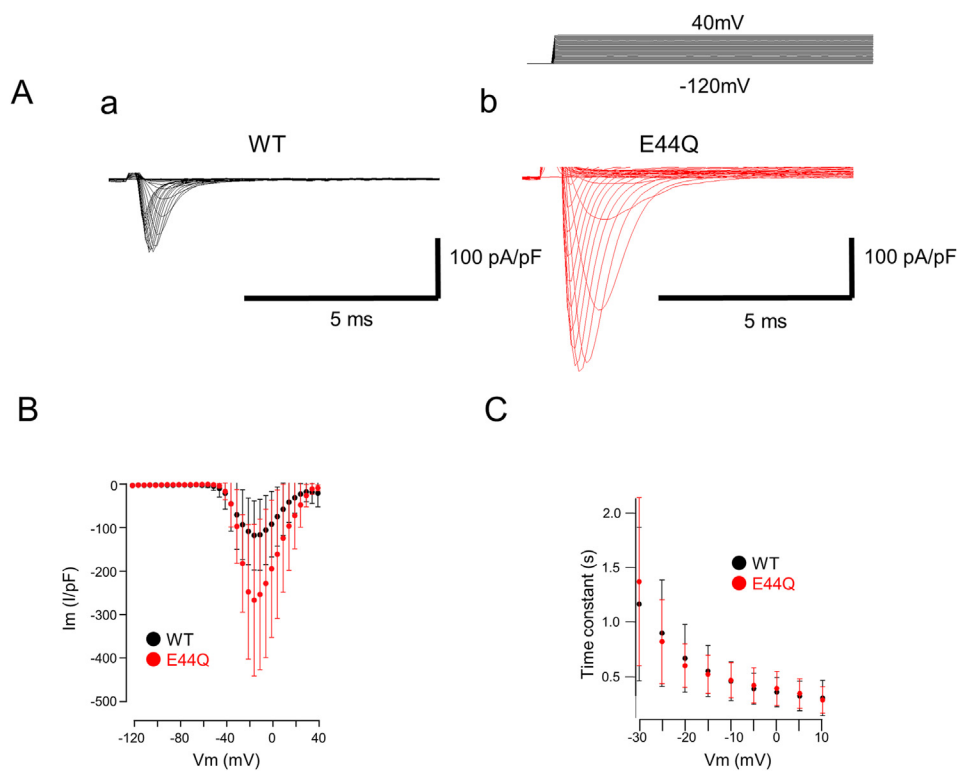
Figure 2. (A) Representative traces from the α subunit of wild-type (WT) and E44Q co-expressed with β1 and β2 subunits in HEK293T cells. (B) Normalized peak current-voltage relationship curves for WT (black circles; n = 9) and E44Q (red circles; n = 8). Im is the peak inward current and Vm is the activation potential. (C) Voltage dependence of fast inactivation time constants for WT (black circles; n = 9) and E44Q (red circles; n = 8). Time constants were calculated from single exponential fits of current decay. The horizontal axis represents activation potentials, and the vertical axis represents time constants.
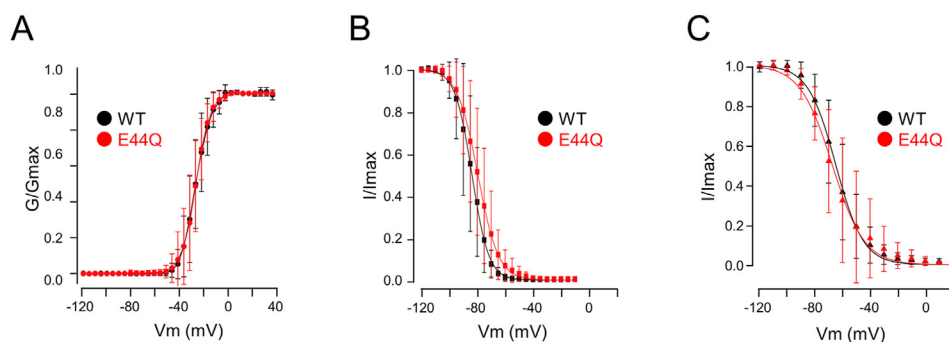
Figure 3. (A) Voltage dependence of activation for wild-type (WT) (black circles; n = 9) and E44Q (red circles; n = 8) Na$_V$1.7. Vm represents the activating pulse potential and G/G$_{max}$ is the sodium conductance normalized to the maximal sodium conductance. Activation curves were derived by fitting Boltzmann functions to the data shown in Figure 2 (B) Steady-state fast inactivation for WT (black squares, n = 9) and E44Q (red squares, n = 10). Vm represents the inactivating prepulse potential, and I/I$_{max}$ represents the peak inward current normalized to the maximal peak current. (C) Steady-state slow inactivation for WT (black squares, n = 8) and E44Q (red squares, n = 8). Vm reflects the inactivating prepulse potential, and I/I$_{max}$ represents the peak inward current normalized to the maximal peak current.

7.9 mV for E44Q (n = 10) (p = 0.253). The slope of the steady-state fast-inactivation relationship was 4.3 ± 0.9 for WT and 5.4 ± 1.7 for E44Q; this difference was not statistically significant (p = 0.121). Figure 3C shows the slow-inactivation curve acquired from the Boltzmann fits to the normalized conductance. The midpoint of steady-state slow inactivation (V$_{1/2}$ measured with 30 s prepulses) was almost similar between WT (−64.1 ± 8.9 mV) and E44Q (−65.1 ± 14.4 mV) (p = 0.529). The slope of the steady-state slow-inactivation relationship was not significantly different (8.7 ± 2.0 for WT and 9.3 ± 3.2 for E44Q; p = 1.000). We then examined the non-inactivating component of the sodium current in WT and E44Q by slow ramp depolarizations (0.2 mV/ms from −100 to 20 mV over 600 ms). It was shown that the amplitude of the current elicited by slow ramp depolarizations for E44Q was significantly larger than that for WT (Figure 4A). We measured the peak amplitude of the inward current elicited by the slow ramp-pulse (Figure 4Ba) and square pulse protocols (Figure 4Bb) and the percentage of the peak ramp current (Figure 4Bc), derived by dividing the former value by the latter value (see Material and Methods). The data varied from cell to cell, and no significant difference was found in the peak inward current amplitudes

between WT and E44Q. In contrast, the percentage of peak current elicited by slow ramp depolarizations was significantly larger for E44Q (−3.25 ± 1.88%, n = 10) than for WT (−1.44 ± 1.09%, n = 10) (p = 0.029; Figure 4Bc). We also measured the voltage showing the peak ramp current (Figure 4Bd). It varied from cell to cell, both for WT and E44Q-mutated channels. It ranged from −50.0 to −21.0 mV (−32.4 ± 12.7 mV, n = 10) for WT and from −47.0 to −8.0 mV (−27.1 ± 13.1 mV, n = 10) for E44Q-mutated channels, and these were not significantly different.

4. Discussion

In this study, we described a novel E44Q mutation in the *SCN9A* gene in a family with paroxysmal pain. Electrophysiologically, the E44Q displayed an increase in the non-inactivating component of the sodium current induced by a ramp-pulse protocol.

Considering the structural and functional characteristics of Na$_V$1.7, most IEM-linked mutations are in (1) the S4, which acts as a voltage sensor; (2) the linker between transmembrane segments S4 and S5 that
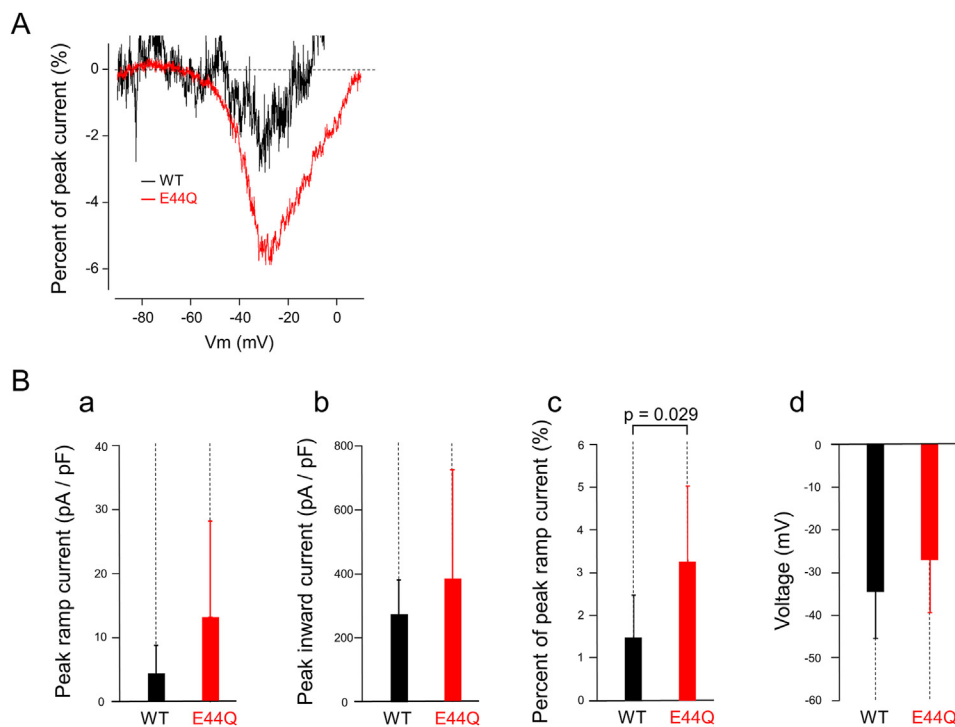
A

B

connects the voltage sensor to the channel pore; and (3) the pore-lining segments of S5 and S6 [2]. Most PEPD-linked mutations are located in the highly conserved inactivation peptide in L3 and the S4–S5 linkers in DIII and DIV [18]. The E44Q mutation, identified in this study, is located in the N-terminus of $Na_V1.7$. This location differs from those of the mutations that cause pain disorders, such as IEM and PEPD. Patch clamp experiments revealed that both the activation and inactivation properties were similar between WT and E44Q, while the non-inactivating component measured by a ramp-pulse protocol was significantly increased in the E44Q. An increase in the non-inactivating component usually accompanies a hyperpolarizing shift in the activation. However, this was not the case in this study (Figure 3). In addition, the voltages reflecting the peak ramp current of the non-inactivating component varied from cell to cell, both in E44Q and WT channels, and were not statistically significant. Thus, the increase in the peak amplitude of the non-inactivating component cannot be explained simply by a possible change in the activation and inactivation gating mechanisms. We have no clear explanation as to why the non-inactivating component was increased, while the activation and inactivation kinetics remained unchanged. In a patient with inherited erythromelalgia with Q10R mutation in the N-terminus of $Na_V1.7$, it has been reported that the mutation caused a hyperpolarizing shift in channel activation [3, 20]. The functional influence of the N-terminus mutation in sodium channel gating conductance has also been reported for other sodium channels [21, 22]. In fact, KIF5B [21] and annexin II light chain (p11) [22] have been shown to interact with the N-terminus of $Na_V1.8$ and promote the translocation of voltage-gated sodium channels to the plasma membrane [23, 24]. Although there are no such reports for $Na_V1.7$, similar regulators may be present, and the interaction between these regulators and the mutants may result in an unexpected effect on channel expression and gating. Thus, it is possible that the newly identified E44Q mutation in the N-terminus of $Na_V1.7$ also affects the voltage-dependent kinetics of the sodium current. $Na_V1.7$ sodium channels play a critical role in determining the excitability threshold of nociceptors and also have an effect on the neurotransmitter release from the central terminals [25]. Thus, we speculate that the increase in ramp current in response to small slow depolarization might amplify small subthreshold stimuli, thus leading to

enhanced excitability in the nociceptor terminals. Further investigation is necessary to confirm this.

In this study, patch clamp recordings were conducted at 25 °C. In clinical practice, patients with E44Q experience episodes of paroxysmal pain that are often induced when the temperature drops, and the pain is relieved by warming. Thus, it may be possible that the $Na_V1.7$ mutation is activated or facilitated by cold temperatures. It should be noted, however, that the temperature inside the body is maintained constant in homeothermic animals even if the temperature of the environment changes, and it is possible that the effects of environmental temperature on the voltage-gated Na channel itself are considerably low. Nevertheless, it will be important to assess the effect of temperature on the gating and conductance of the $Na_V1.7$ channel and its mutation in future studies.

Our patient experienced paroxysmal extremity pain in childhood and trigeminal neuralgia in adulthood, both of which were triggered by cold stimuli. The extremity pain was induced by cold and relieved by warming. It disappeared temporarily during adolescence. These characteristics were more similar to FEP in patients with an SCN11A mutation than IEM in patients with an SCN9A mutation, the latter being characterized by burning pain induced by warmth and relieved by cooling [7, 8, 10]. Therefore, screening for SCN9A mutations should be performed even if pain episodes resemble SCN11A-related FEP. In addition, trigeminal neuralgia is often triggered by gentle touching of the face and talking [26]. There are few reports of trigeminal neuralgia being triggered by low temperatures [27]. Since Aδ and C fibers, which express $Na_V1.7$, are activated by noxious cold stimuli [28], cold sensation and the E44Q mutation might have a synergistic effect in trigeminal neuralgia.

In conclusion, we report a novel E44Q mutation in the SCN9A gene in a family with paroxysmal pain. Early symptoms were similar to those of SCN11A-related FEP. Electrophysiological analyses indicated that E44Q is a gain-of-function $Na_V1.7$ mutation, which is consistent with the pain phenotype of the proband. A genetic analysis of SCN9A and SCN10A, as well as of SCN11A, is necessary for patients with familial pain disorders, even if the symptoms are similar to those of FEP associated with the SCN11A mutation.

Declarations

Data availability statement

The data that has been used is confidential.

Declaration of interests statement

The authors declare the following conflict of interests:

Akio Koizumi; Reports personal fees from AlphaNavi Pharma during the study period.

Hiroko Okuda; Reports grants from AlphaNavi Pharma during the study period.

Atsuko Noguchi, Tsutomu Takahashi, Akio Koizumi, Hatasu Kobayashi and Kouji H. Harada; Have a patent-pending regarding SCN11A (name of patent, 'Pain gene and its applications'; Japanese Patent Application No. P2016-098215A).

Additional information

No additional information is available for this paper.

References

[1] A.L. Hodgkin, A.F. Huxley, A quantitative description of membrane current and its application to conduction and excitation in nerve, J. Physiol. 117 (1952) 500–544.

[2] D.L. Bennett, A.J. Clark, J. Huang, et al., The role of voltage-gated sodium channels in pain signaling, Physiol. Rev. 99 (2019) 1079–1151.

[3] S.G. Waxman, I.S.J. Merkies, M.M. Gerrits, et al., Sodium channel genes in pain-related disorders: phenotype–genotype associations and recommendations for clinical use, Lancet Neurol. 13 (2014) 1152–1160.

[4] S.D. Dib-Hajj, Y. Yang, J.A. Black, et al., The Na(V)1.7 sodium channel: from molecule to man, Nat. Rev. Neurosci. 14 (2013) 49–62.

[5] C. Han, J. Huang, S.G. Waxman, Sodium channel Nav 1.8: emerging links to human disease, Neurology 86 (2016) 473–483.

[6] S.D. Dib-Hajj, J.A. Black, S.G. Waxman, NaV1.9: a sodium channel linked to human pain, Nat. Rev. Neurosci. 16 (2015) 511–519.

[7] R. Kabata, H. Okuda, A. Noguchi, et al., Familial episodic limb pain in kindreds with novel Nav 1.9 mutations, PloS One 13 (2018), e0208516.

[8] H. Okuda, A. Noguchi, H. Kobayashi, et al., Infantile pain episodes associated with novel Nav 1.9 mutations in familial episodic pain syndrome in Japanese families, PloS One 11 (2016), e0154827.

[9] P.J. van Genderen, J.J. Michiels, J.P. Drenth, Hereditary erythermalgia and acquired erythromelalgia, Am. J. Med. Genet. 45 (1993) 530–532.

[10] J.P. Drenth, S.G. Waxman, Mutations in sodium-channel gene SCN9A cause a spectrum of human genetic pain disorders, J. Clin. Invest. 117 (2007) 3603–3609.

[11] R. Hayden, M. Grossman, Rectal, ocular, and submaxillary pain; a familial autonomic disorder related to proctalgia fugaz: report of a family, AMA J. Dis. Child. 97 (1959) 479–482.

[12] C.R. Fertleman, C.D. Ferrie, What's in a name-familial rectal pain syndrome becomes paroxysmal extreme pain disorder, J. Neurol. Neurosurg. Psychiatry 77 (2006) 1294–1295.

[13] T.R. Cummins, S.D. Dib-Hajj, S.G. Waxman, Electrophysiological properties of mutant Nav 1.7 sodium channels in a painful inherited neuropathy, J. Neurosci. 24 (2004) 8232–8236.

[14] S.D. Dib-Hajj, A.M. Rush, T.R. Cummins, et al., Gain-of-function mutation in Nav 1.7 in familial erythromelalgia induces bursting of sensory neurons, Brain 128 (2005) 1847–1854.

[15] C. Han, A.M. Rush, S.D. Dib-Hajj, et al., Sporadic onset of erythermalgia: a gain-of-function mutation in Nav 1.7, Ann. Neurol. 59 (2006) 553–558.

[16] T.P. Harty, S.D. Dib-Hajj, L. Tyrrell, et al., Na(V)1.7 mutant A863P in erythromelalgia: effects of altered activation and steady-state inactivation on excitability of nociceptive dorsal root ganglion neurons, J. Neurosci. 26 (2006) 12566–12575.

[17] A. Lampert, S.D. Dib-Hajj, L. Tyrrell, et al., Size matters: erythromelalgia mutation S241T in Nav 1.7 alters channel gating, J. Biol. Chem. 281 (2006) 36029–36035.

[18] C.R. Fertleman, M.D. Baker, K.A. Parker, et al., SCN9A mutations in paroxysmal extreme pain disorder: allelic variants underlie distinct channel defects and phenotypes, Neuron 52 (2006) 767–774.

[19] S.D. Dib-Hajj, M. Estacion, B.W. Jarecki, et al., Paroxysmal extreme pain disorder M1627K mutation in human Nav 1.7 renders DRG neurons hyperexcitable, Mol. Pain 4 (2008) 37.

[20] C. Han, S.D. Dib-Hajj, Z. Lin, et al., Early- and late-onset inherited erythromelalgia: genotype-phenotype correlation, Brain 132 (2009) 1711–1722.

[21] K. Okuse, M. Malik-Hall, M.D. Baker, et al., Annexin II light chain regulates sensory neuron-specific sodium channel expression, Nature 417 (2002) 653–656.

[22] Y.Y. Su, M. Ye, L. Li, et al., KIF5B promotes the forward transport and axonal function of the voltage-gated sodium channel Nav 1.8, J. Neurosci. 33 (2013) 17884–17896.

[23] C. Lossin, A catalog of SCN1A variants, Brain Dev. 31 (2009) 114–130.

[24] D.L. Bennett, C.G. Woods, Painful and painless channelopathies, Lancet Neurol. 13 (2014) 587–599.

[25] D.J. Tester, M.L. Will, C.M. Haglund, et al., Compendium of cardiac channel mutations in 541 consecutive unrelated patients referred for long QT syndrome genetic testing, Heart Rhythm. 2 (2005) 507–517.

[26] G. Di Stefano, S. Maarbjerg, T. Nurmikko, et al., Triggering trigeminal neuralgia, Cephalalgia 38 (2018) 1049–1056.

[27] W. Koh, H. Lim, X. Chen, Atypical triggers in trigeminal neuralgia: the role of A-delta sensory afferents in food and weather triggers, Korean J. Pain 34 (2021) 66–71.

[28] R.J. Schepers, M. Ringkamp, Thermoreceptors and thermosensitive afferents, Neurosci. Biobehav. Rev. 34 (2010) 177–184.